

# CuO and ZnO nanoparticles: phytotoxicity, metal speciation, and induction of oxidative stress in sand-grown wheat

Christian O. Dimkpa · Joan E. McLean · Drew E. Latta · Eliana Manangón · David W. Britt · William P. Johnson · Maxim I. Boyanov · Anne J. Anderson

Received: 17 September 2011 / Accepted: 10 August 2012 / Published online: 21 August 2012  
© Springer Science+Business Media B.V. 2012

**Abstract** Metal oxide nanoparticles (NPs) are reported to impact plant growth in hydroponic systems. This study describes the impact of commercial CuO (<50 nm) and ZnO (<100 nm) NPs on wheat (*Triticum aestivum*) grown in a solid matrix, sand. The NPs contained both metallic and non-metallic impurities to different extents. Dynamic light scattering and atomic force microscopy (AFM) assessments confirmed aggregation of the NPs to submicron sizes. AFM showed transformation of ZnO NPs from initial rhomboid shapes in water to elongated rods in the aqueous phase of the sand matrix. Solubilization of metals occurred in the sand at similar rates from CuO or ZnO NPs as their

bulk equivalents. Amendment of the sand with 500 mg Cu and Zn/kg sand from the NPs significantly ( $p = 0.05$ ) reduced root growth, but only CuO NPs impaired shoot growth; growth reductions were less with the bulk amendments. Dissolved Cu from CuO NPs contributed to their phytotoxicity but Zn release did not account for the changes in plant growth. Bioaccumulation of Cu, mainly as CuO and Cu(I)-sulfur complexes, and Zn as Zn-phosphate was detected in the shoots of NP-challenged plants. Total Cu and Zn levels in shoot were similar whether NP or bulk materials were used. Oxidative stress in the NP-treated plants was evidenced by increased lipid peroxidation and oxidized glutathione in roots and decreased chlorophyll content in shoots; higher peroxidase and catalase activities were present in roots. These findings correlate with the NPs causing increased production of reactive oxygen species. The accumulation of Cu and Zn from NPs into edible plants has relevance to the food chain.

C. O. Dimkpa · D. W. Britt · A. J. Anderson  
Department of Biological Engineering,  
Utah State University, Logan, UT 84322, USA

C. O. Dimkpa (✉) · A. J. Anderson  
Department of Biology, Utah State University,  
Logan, UT 84322, USA  
e-mail: cdimkpa@usu.edu

J. E. McLean  
Utah Water Research Laboratory, Utah State University,  
Logan, UT 84322, USA

D. E. Latta · M. I. Boyanov  
Biosciences Division, Argonne National Laboratory,  
Argonne, IL 60439, USA

E. Manangón · W. P. Johnson  
Department of Geology and Geophysics,  
University of Utah, Salt Lake City, UT 84112, USA

**Keywords** Environmental health and safety · Metal bioaccumulation · Metal speciation · Metal oxide nanoparticles · Oxidative stress · Phytotoxicity · Solid growth matrix · Wheat

## Introduction

Recent advances in nanotechnology include the incorporation of metallic nanoparticles (NPs) into

diverse industrial, medical, and household products (Lee et al. 2008, 2010; Navarro et al. 2008). Improper handling and disposal of NP-containing wastes could result in environmental contamination. NPs have the potential for harmful effects on plants and plant-associated soil bacteria (Dimkpa et al. 2011a, b; Du et al. 2011; Gajjar et al. 2009; Lin and Xing 2007, 2008; Nair et al. 2010; Stampoulis et al. 2009). At sublethal concentrations, NPs variably modify the production of bacterial secondary metabolites involved in plant growth and productivity (Dimkpa et al. 2012a, b, c).

The accumulation from NPs of metals at high levels in the plant could not only impact their growth, but could pose a route for contamination of the food chain. Growth of food plants such as cucumber, lettuce, bean, corn, rye, and zucchini is impaired, depending on the concentration of NPs of Ag, Cu, CuO, TiO<sub>2</sub>, Zn, and ZnO (Asli and Neumann 2009; Atha et al. 2012; Barrena et al. 2009; Du et al. 2011; Lin and Xing 2007, 2008; Stampoulis et al. 2009). However, Ni(OH)<sub>2</sub> NPs do not effect growth of mesquite (Parsons et al. 2010), while in spinach, TiO<sub>2</sub> NPs increase rubisco activase to enhance photosynthesis and plant growth (Gao et al. 2006, 2008). Toxicity of NPs depends on conformation, surface characteristics, such as the presence of coatings, and their aggregation state (Barrena et al. 2009; Pal et al. 2007; Yang and Watts 2005). Triangle-shaped Ag NPs are more bioactive than spherical ones (Pal et al. 2007).

Intact ZnO NPs are observed within hydroponically grown plant roots (Lin and Xing, 2008), and uptake into shoots is observed for other NPs (Lee et al. 2008; Parsons et al. 2010; Zhang et al. 2011; Zhu et al. 2008). Disruption of water- and nutrient-transport pathways is one mechanism proposed to account for how the NPs cause plant damage (Asli and Neumann 2009; Lin and Xing 2008). In addition, the metallic NPs may release soluble metals (Dimkpa et al. 2011a, b; Lee et al. 2008; Lin and Xing 2008; Stampoulis et al. 2009; Wang et al. 2011) that are taken up by the plant. Indeed, exposure to ions of Al, Cd, Cu, Fe, Mn, Ni, Zn, and U results in an array of symptoms including increased lipid membrane peroxidation, loss of chlorophyll pigmentation, altered ferric iron metabolism, modification in the activities of stress-inducible enzymes and levels of plant growth regulators (Dimkpa et al. 2008, 2009; Panda et al. 2003; Potters et al. 2007). Potters et al. (2007) coined the phrase “generic

stress-induced modification of plant morphology” to account for the similarity in response to heavy metals and other abiotic challenges.

The NP-plant studies described above were conducted under hydroponic systems. In contrast, the studies presented in this paper evaluated the impact of commercially available NPs of CuO and ZnO on growth, metal bioaccumulation, and metabolic processes in wheat (*Triticum aestivum*) grown in sand. This solid matrix will provide a more representative indication of the impact of NPs on plants under environmentally relevant conditions.

## Materials and methods

### Sources of CuO and ZnO nano and bulk particles

CuO NPs (particle size <50 nm) and ZnO NPs (<100 nm), as well as bulk CuO (8,000–9,000 nm) and bulk ZnO (<1,000 nm) were obtained from Sigma-Aldrich, MO, USA.

### Characterization of sand matrix

Commercial white silica sand (UNIMIN Corp., ID, USA) was sieved for particle sizing and washed thoroughly with water before drying and use. To determine the presence of water-soluble trace elements in the sand that may contribute to plant growth performance, 20 g (wet weight) of sand was extracted with 40 ml of deionized water for 24 h on a reciprocal shaker. Extractions were performed in triplicate. The aqueous fraction was filtered through a 0.2- $\mu$ m filter and analyzed for elemental content using inductively coupled mass spectroscopy (ICP-MS) (Agilent 7500c), for major cations by ion chromatography (Dionex ICS-3000) and specific conductance. Organic and inorganic carbon content of the sand was determined using Skalar Primacs-SLC TOC Analyser (Skalar Analytical, Netherlands).

Characterization of CuO and ZnO NPs: determination of chemical impurities, size distribution, atomic force microscopy, and dissolution

The presence of elemental impurities in the commercial NP products was determined by dissolving 0.2 g

CuO and ZnO NPs in 20 ml 50 % nitric acid. The ZnO NPs dissolved without heating; the CuO NPs in acid were gently heated on a hot plate until the particles dissolved. Samples were diluted to 100 ml with deionized water and analyzed using ICP-MS. NP size was determined by dynamic light scattering (DLS) using a DynaPro NanoStar (Wyatt Technology Corporation, Santa Barbara, CA) as described previously (Dimkpa et al. 2012c). For imaging of the NPs, sand (40 g) was washed in water, dried and then mixed with NPs to a concentration of 500 mg metal/kg sand. The sand–NP mix was moistened with 10 ml of double distilled (dd) H<sub>2</sub>O and shaken thoroughly to ensure even mixing. After 14 h of equilibration, the upper aqueous layer was removed. Samples of this material as well as freshly prepared stocks of the NPs in H<sub>2</sub>O were dried onto a mica surface for imaging by atomic force microscopy (AFM) using published procedures (Dimkpa et al. 2011a). As a control, the H<sub>2</sub>O-fraction from sand treated with H<sub>2</sub>O but lacking NPs was imaged.

Metal solubility was determined following exposure of NPs and bulk particles of CuO and ZnO in sand at 0, 1, 7, and 14 days (d). These time periods were chosen based on the 14-d plant growth period. The sand (300 g) was mixed thoroughly with 500 mg Cu or Zn/kg sand from CuO and ZnO NPs and bulk materials, and 40 g aliquots transferred to 50-ml centrifuge tubes followed by the addition of 11.1 ml of dd-H<sub>2</sub>O to saturate the matrix. The samples were tumbled for 1 h before immediate assay or further incubation without shaking at room temperature for 1, 7, and 14 d. At sampling, the samples were extracted with 10 ml of dd-H<sub>2</sub>O followed by shaking for 1 h, centrifugation at 10,000g for 10 min, and recovery of the H<sub>2</sub>O layer from the top of the samples. This aqueous layer was recentrifuged for 30 min at 15,557 g to pellet NPs (Dimkpa et al. 2011b). The supernatants were transferred to test tubes and analyzed by ICP-MS for soluble Cu and Zn contents. Sand-lacking NP treatment but treated with H<sub>2</sub>O was assayed only at d 14. Three replicate analyses were performed for all treatments.

#### Plant growth conditions

Sand (300 g) was sterilized in closed transparent Magenta boxes by autoclaving, and then amended with 500 mg/kg of Cu or Zn from CuO and ZnO NPs

or bulk materials and mixed before adding 75 ml deionized H<sub>2</sub>O; only H<sub>2</sub>O was added for the control studies. Food-grade organic winter wheat berries were surface-sterilized in 10 % hydrogen peroxide (H<sub>2</sub>O<sub>2</sub>) for 15 min and rinsed thoroughly in autoclaved dd-H<sub>2</sub>O. Three wheat seeds were sown at separate locations per box at depths of about 0.5 cm. Seedlings were grown under fluorescent growth lights at 28 °C for 14 d before harvesting and analyses. No nutrient solutions were added to avoid speciation of metals from the NPs and bulks with nutrient components. To evaluate the role of dissolved Cu and Zn from CuO and ZnO NPs in wheat growth inhibition, the ion equivalent [from CuCl<sub>2</sub> and Zn(NO<sub>3</sub>)<sub>2</sub>] of the highest levels of Cu (3 mg Cu/kg sand) and Zn (7 mg Zn/kg sand) dissolved from the respective metal products in sand were used in plant growth. Root and shoot length, and number of roots originating from the stem base, were recorded. Where necessary, the roots and shoots were stored frozen until assayed for cellular activity.

#### Determination of lipid membrane peroxidation and enzyme activities in roots of NP-treated plant

Root lipid membrane peroxidation was determined by the thiobarbituric acid assay which measures the amount of malondialdehyde (MDA) (Cakmak and Horst 1991). Extracts were prepared from portions of fresh roots, and MDA content was measured colorimetrically following methods described in Cakmak and Horst (1991) and Dimkpa et al. (2009). For enzyme activity assays, portions of the root samples (1.0 g) were extracted in 50 mM Tris–HCl buffer (pH 7.5), consisting of 5 mM EDTA, 1 % phenylmethylsulfonyl fluoride, 10 mM dithiothreitol, and 3 % insoluble polyvinylpyrrolidone (Márquez-García and Córdoba 2009). The cell debris in the extracts was removed by centrifugation at 10,000g for 20 min. Peroxidase (POD) activity was determined using the chromogenic substrate 4-chloronaphthol (4-CN; Sigma-Aldrich, St Louis, MO, USA) from procedures modified from Akiyama et al. (1989). Supernatants from the extracts (100 µl) were added to reaction mixtures of one ml containing 4-CN (3 mg), sodium phosphate buffer (0.1 M; 10 ml; pH 7.4) and 3 % H<sub>2</sub>O<sub>2</sub> (0.1 ml). After 5 min, the color formation was measured spectrophotometrically at 570 nm. Catalase (CAT) activity was determined by the method of Akiyama et al. (1989) with the addition of extracts

(100  $\mu\text{l}$ ) to a 1 ml buffer containing 50 mM Tris–HCl (pH 7.5) and 10 mM  $\text{H}_2\text{O}_2$ , and following the decomposition of  $\text{H}_2\text{O}_2$  at 240 nm. CAT activity was calculated based on the published extinction coefficient of  $\text{H}_2\text{O}_2$  at 240 nm,  $43.6 \text{ mM}^{-1}$  (Márquez-García and Córdoba 2009). All assays were performed using five different plant samples from two independent studies.

#### Evaluation of IAA and glutathione oxidation in roots and shoots of NP-treated plants

The potential oxidation of IAA by IAA oxidase was evaluated according to previously described procedures (Dimkpa et al. 2009). The method involves using the colorimetric test with Salkowski's reagent to detect the level of IAA after incubation with plant extracts and 2,4-dichlorophenol and  $\text{MnCl}_2$ . Authentic IAA was used to prepare a standard curve for calculation of residual auxin levels. The presence of oxidized glutathione (GSSG) in the plant shoots and roots was detected using the GSSG-Glo Glutathione Assay kit (Promega, WI, USA) according to the manufacturer's protocol. Briefly, supernatants from root or shoot extracts (50  $\mu\text{l}$ ) of control and NP-treated plants, prepared in Tris–HCl buffer as described above, were transferred to a 96-well plate, each in triplicate, and 50  $\mu\text{l}$  GSH-Glo reagent  $2\times$  [containing luciferin-NT [15  $\mu\text{l}$ ], glutathione-S-transferase (15  $\mu\text{l}$ ), and the GSH-Glo reagent buffer (0.8 ml)]. The mixture was incubated for 30 min at room temperature, when 100  $\mu\text{l}$  of a reconstituted Luciferin Detection Reagent (Promega, WI, USA) was added, followed by a further incubation for 15 min. Luminescence was recorded using a LMAXII Luminometer (Molecular Devices Corporation, Sunnyvale CA), with a 10 s exposure. All assays were from five different plant samples from two independent growth studies.

#### Measurement of chlorophyll contents

Chlorophyll was extracted in dimethylsulfoxide from shoots according to the procedure of Tait and Hik (2003). Absorbance measurements at 665 and 649 nm permitted the calculation of the total chlorophyll content using published formula (Tait and Hik 2003). Assays were from five different plant samples from two independent growth studies.

#### Determination of Cu and Zn accumulation and speciation in shoot from NPs

Shoots from 15 replicates of three independent growth studies for control and NP- and bulk-treated plants were harvested with care to eliminate contamination with the growth matrix. Shoots from each treatment of the same study were pooled, dried, digested with  $\text{HNO}_3$ , and analyzed for their Cu and Zn contents using ICP-MS. For determination of metal speciation in the NP-treated plants, samples were prepared by grinding freeze-dried shoots with a mortar and pestle and placing the powders in drilled plastic slides covered with Kapton film windows. Ambient-temperature Cu and Zn K-edge X-ray absorption near-edge spectroscopy (XANES) measurements were performed at the MRCAT/Enviro-CAT sector 10-BM bending magnet beam line, Advanced Photon Source (APS) Argonne National Laboratory, Argonne IL (Kropf et al. 2010). Data were collected in fluorescence mode using a Stearn-Heald type detector (Stearn and Heald 1979). Previous studies reported radiation-induced reduction of Cu in hydrated samples (Manceau and Matynia 2010; Pokrovsky et al. 2012). In our study, radiation-induced changes in Cu or Zn speciation in the samples were monitored by comparing successive XANES scans at freshly irradiated locations on the sample. No differences were observed on the time-scale of a XANES scan ( $\sim 10$  min) and over extended periods of irradiation (8–10 h). Factors that may have contributed to the lack of evolution in the Cu XANES spectra on the timescale of our measurements include freeze-drying of the shoot samples and the relatively low photon density of the X-ray beam. Energy calibration was maintained during all scans by simultaneous collection of XANES data from Cu or Zn metal foils using X-rays transmitted through the samples. Standards used in Cu K-edge XANES analysis are the commercial CuO NPs,  $\text{Cu}_2\text{O}$ , CuS,  $\text{Cu}_2\text{S}$ , aqueous and solid Cu(II)-acetate,  $\text{Cu}_2(\text{OH})\text{PO}_4$ ,  $\text{CuSO}_4\cdot 5\text{H}_2\text{O}$ , a Cu–cysteine/cystine complex. Standards used for the Zn k-edge XANES analysis are: commercial ZnO NPs, ZnS, aqueous Zn-acetate, an aqueous Zn–cysteine complex, and  $\text{Zn}_3(\text{PO}_4)_2\cdot 4\text{H}_2\text{O}$ . Data processing and linear combination (LC) XANES analysis were done in the software program ATHENA (Newville 2001; Ravel and Newville 2005).

Statistical analysis

An analysis of variance (ANOVA) determined if there were significant differences in replicated data, and where significant, treatments were separated by the Tukey’s test using the OriginPro 8.1 statistical software.

Results

Characterization of sand matrix

The elemental content of the water extraction of the sand matrix used in the study can be found in Table 1; there is no evidence of trace contamination. The specific conductance of the solution was 28 μS/cm, equivalent to an ionic strength of  $2 \times 10^{-4}$  M, with 4.0 mg Na/l and <1.0 mg/l of K, Ca, and Mg present. The sand is 99 % quartz, 84 % of coarse to very coarse texture; no fine or very fine sand was detectible. In addition, no organic carbon or carbonate minerals were detected.

Impurity levels of commercial CuO and ZnO NPs and their size distribution and atomic force microscopy in water suspensions

The elemental composition and total amounts of impurities in the commercial CuO and ZnO NPs are listed in Table 1. The CuO NPs are contaminated with metals and Si and P presumably as oxyanions ( $\text{SiO}_4^{4-}$  and  $\text{PO}_4^{3-}$ ); the ZnO NPs had lesser contamination with Si and P. Concentrations of metallic impurities were very low, relative to the amounts of Cu or Zn. Except for cadmium, the CuO NPs contained higher concentrations of the respective elemental impurities than the ZnO NPs. Suspensions of the CuO and ZnO NPs in H<sub>2</sub>O formed aggregates with sizes more than 100 nm when assayed by DLS; the size range was greater for the ZnO NPs than the CuO NPs (Fig. 1). Fractions of size around 300 nm agreed with our published data where particle size was judged by field flow fractionation (Gajjar et al. 2009). AFM imaging confirmed aggregation of these NPs but also showed both NPs contained materials <100 nm, confirming previous reports (Dimkpa et al. 2011b). Exposure to the sand matrix for 14 h resulted in

**Table 1** Elemental composition in soluble water washes from the sand used as the plant growth matrix and impurities obtained in an acid digestion of the commercial CuO and ZnO NPs

| Element    | Concentration in sand (μg/g) | Concentration in CuO NPs (μg/g) | Concentration in ZnO NPs (μg/g) |
|------------|------------------------------|---------------------------------|---------------------------------|
| Aluminum   | 0.71 ± 0.11                  | 216 ± 23.0                      | 1.58 ± 0.45                     |
| Antimony   | <7 × 10 <sup>-4</sup>        | 1.99 ± 0.42                     | <0.17                           |
| Arsenic    | 0.003 ± 0.0003               | 17.5 ± 0.4                      | <0.1                            |
| Barium     | 0.02 ± 0.004                 | 3.05 ± 0.24                     | <0.29                           |
| Beryllium  | <2 × 10 <sup>-4</sup>        | 0.13 ± 0.01                     | <0.06                           |
| Cadmium    | <4 × 10 <sup>-4</sup>        | 0.46 ± 0.01                     | 1.44 ± 0.008                    |
| Cobalt     | <8 × 10 <sup>-4</sup>        | 86.3 ± 1.5                      | <0.17                           |
| Chromium   | <5 × 10 <sup>-4</sup>        | 18.5 ± 5.4                      | <0.1                            |
| Copper     | <5 × 10 <sup>-3</sup>        | 694,000 ± 22,000                | <1.2                            |
| Lead       | 4.19 × 10 <sup>-4</sup>      | 4.43 ± 0.61                     | 5.13 ± 0.04                     |
| Iron       | 0.1 ± 0.05                   | 814 ± 41                        | 4.45 ± 1.43                     |
| Manganese  | <0.01                        | 130 ± 3.0                       | <0.43                           |
| Nickel     | <8 × 10 <sup>-4</sup>        | 18.3 ± 9.0                      | <0.2                            |
| Phosphorus | NA                           | 137 ± 0.65                      | 27.5 ± 0.85                     |
| Selenium   | <3 × 10 <sup>-4</sup>        | 0.76 ± 0.16                     | <0.1                            |
| Silicon    | NA                           | 500 ± 91                        | 4.46 ± 0.7                      |
| Thallium   | <3 × 10 <sup>-4</sup>        | 0.13 ± 0.01                     | <0.06                           |
| Vanadium   | 0.015 ± 0.0006               | 7.45 ± 0.11                     | <0.15                           |
| Zinc       | <1.0 × 10 <sup>-2</sup>      | 153 ± 42.4                      | 788,000 ± 55,000                |

NA not analyzed

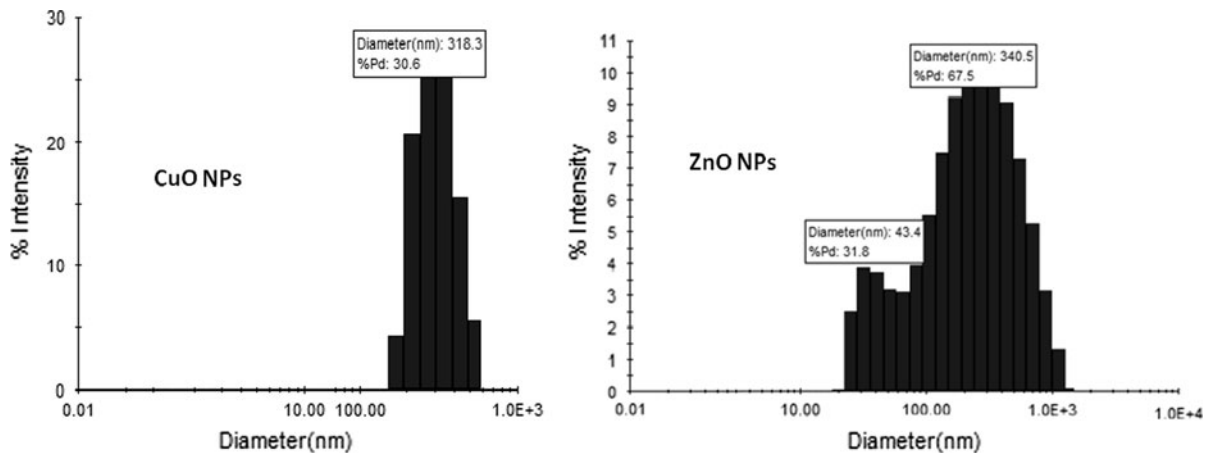


**Fig. 1** Size distribution of CuO and ZnO NPs (500 mg metal/l) in water suspensions. Data are from two different DLS measurements

aggregation of the CuO NPs to larger-sized particles than particles prepared just in water (Fig. 2a vs. c). For the ZnO NPs, a transition from angular structures to

elongated rods over a micron in length was observed (Fig. 2b vs. d). No particles of similar size or shape as the NPs were evident when samples of H<sub>2</sub>O from

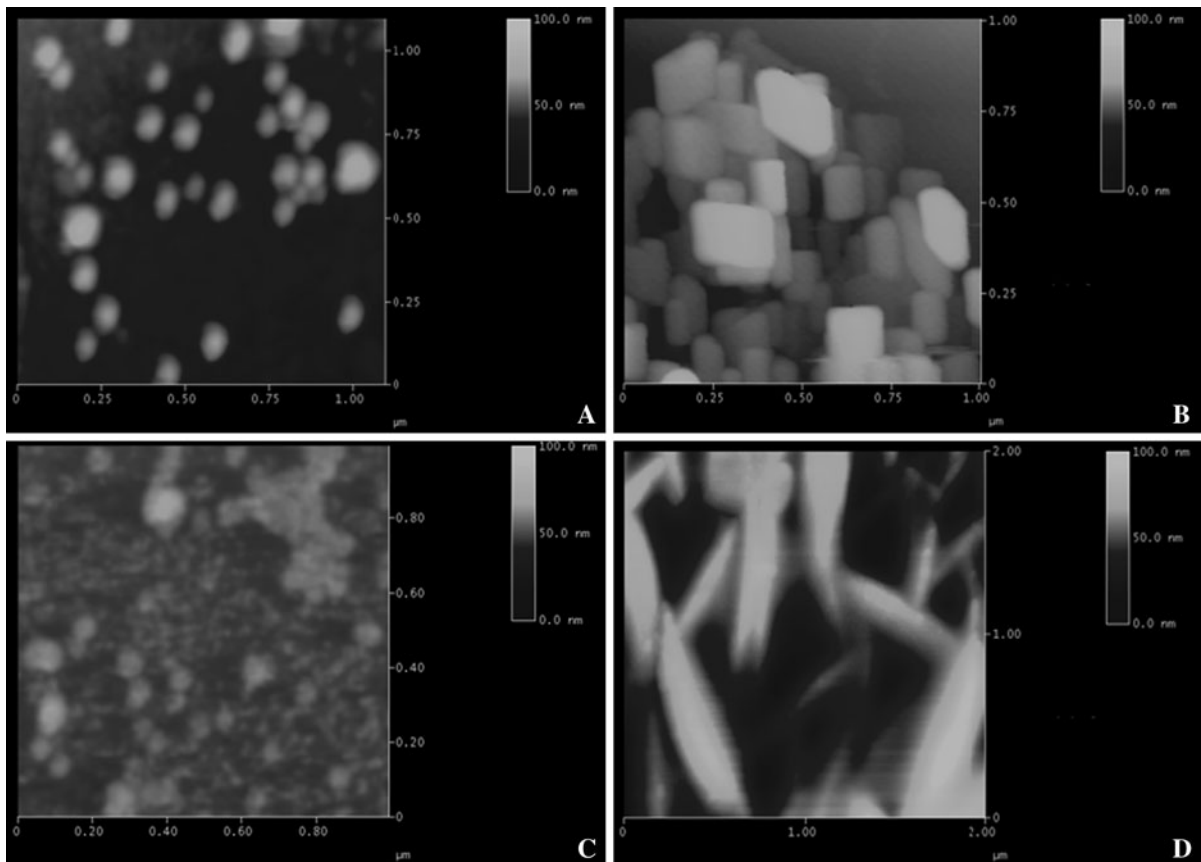


**Fig. 2** Topographical atomic force microscopy images indicating height bars for **a** CuO NPs, **b** ZnO NPs, from water suspensions of 500 mg metal/l, and **c** CuO NPs, and **d** ZnO NPs, after exposure as a sand (500 mg metal/kg sand)–water mix for 14 h

sand not amended with NPs were imaged (data not shown).

#### Solubilization of metals from CuO and ZnO NPs and bulks in wetted sand

Metals contributed by the sand in the growth boxes (pH 7.9) were 0.023 mg Cu/l and 0.061 mg Zn/l. Metal release from the NPs and bulk materials was time dependent (Fig. 3). Solubility from the CuO NPs and bulk was the same statistically, except for the 0 h time; levels did not exceed 3 mg/l Cu. Solubility of Zn was highest at 24 h for ZnO NPs (5 mg/l) and immediately after suspension for the ZnO bulk material (7 mg/l), with values falling to less than 3 mg/l in both cases at d 7 and 14.

#### Growth of wheat in sand amended with CuO and ZnO NPs and bulks

By 14 d of seedling development, root growth was more impacted by the metal products than shoot growth. Shoot length was reduced significantly ( $p = 0.05$ ) by 13 % by CuO NPs, and there was a trend for reduced (8 % decrease) shoot length with ZnO NPs (Table 2). Both NPs significantly ( $p = 0.05$ ) reduced root length, 59 % for the CuO NPs, and 53 % for the ZnO NPs. In contrast to plant length (root and shoot), both CuO NPs and ZnO NPs caused proliferation of the number of the roots significantly ( $p = 0.05$ ) increasing the number of roots by 42 and 35 %, respectively (Table 2). Roots of the CuO NP-

treated plants had brown necrotic lesions, and were thinner and more brittle than the control plants. Growth effects were less with the bulk materials: shoot length was unaffected, although root length was reduced significantly ( $p = 0.05$ ) by bulk CuO (32 %) and by bulk ZnO (34 %). Root number also was affected by the bulk products, with a significant ( $p = 0.05$ ) increase of 42 % for treatment with CuO, and an insignificant increase of 19 % with ZnO. Neither bulk CuO nor ZnO NPs had a significant impact on plant biomass. Bulk ZnO increased plant biomass significantly ( $p = 0.05$ ) by 38 % and CuO NP treatments 75 %, from the control.

#### Shoot bioaccumulation of Cu and Zn from CuO and ZnO NPs and bulks

As anticipated from the essential metabolic roles of Cu and Zn, both metals were detected by ICP-MS analysis in digests from shoots of the control plants ( $19 \pm 8$  mg Cu/kg, and  $88 \pm 23$  mg Zn/kg shoot dry weight). Levels increased significantly ( $p = 0.05$ ) by the same amount when plants were grown with the NP or the bulk materials:  $375 \pm 115$  mg Cu/kg shoot dry weight with CuO NPs,  $254 \pm 165$  mg Cu/kg shoot dry weight with bulk CuO, and  $2076 \pm 670$  mg Zn/kg shoot dry weight with ZnO NPs and  $2138 \pm 943$  mg Zn/kg shoot dry weight with bulk ZnO. There was significantly ( $p = 0.05$ ) more Zn in the shoots than Cu.

#### Speciation of Cu and Zn in wheat shoot

The Cu XANES measurements are shown in Fig. 4a. Cu XANES spectra have features that allow distinction between Cu(II), Cu(I), and Cu(0) valence states, as well as between Cu–O and Cu–S coordination (Kau et al. 1987; Manceau and Matynia 2010; Pokrovsky et al. 2012). The XANES of shoots grown with CuO NPs had a spectrum similar to that of the starting CuO NPs; however, the spectrum from the shoots had a slightly attenuated white line intensity ( $\sim 8,998$  eV), and a shoulder feature at 8,981 eV. The latter features resulted from the presence of Cu(I) (Kim et al. 2003; Manceau and Matynia 2010; Pokrovsky et al. 2012). LC fits of the spectrum with the standards spectra on Fig. 4a indicated that the majority ( $64 \pm 10$  %) of the measured Cu spectrum was reproduced by the spectrum of the CuO NPs. The spectra from bulk CuO and

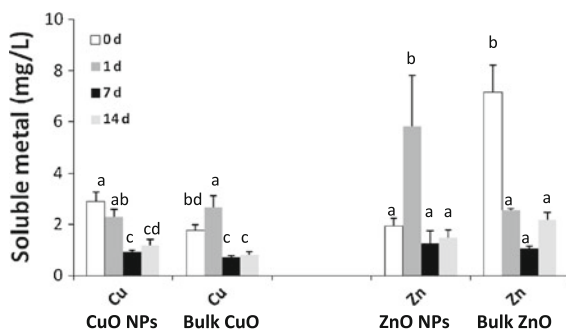


**Fig. 3** Solubility of Cu from CuO NPs and bulk CuO, and Zn from ZnO NPs, and bulk ZnO (each at 500 mg metal/kg) after exposure to sand for 0, 1, 7, and 14 d. Values are mean, and SD of three replications and *different letters* indicate significant differences ( $p = 0.05$ ) compared differently between CuO NPs and bulk CuO or ZnO and bulk ZnO across all time points

**Table 2** Growth responses of wheat plants grown for 14 days in a sand matrix amended with CuO and ZnO NPs and bulk CuO and ZnO at 500 mg metal/kg

| Treatment | Growth response   |                  |             |                                  |
|-----------|-------------------|------------------|-------------|----------------------------------|
|           | Shoot length (cm) | Root length (cm) | Root number | Plant biomass [root + shoot (g)] |
| Control   | 18.4 ± 4.0a       | 10.2 ± 2.8a      | 5.2 ± 1.3a  | 0.08 ± 0.03ab                    |
| CuO NPs   | 16.0 ± 3.0b       | 4.2 ± 2.1b       | 7.4 ± 1.4b  | 0.06 ± 0.03a                     |
| Bulk CuO  | 18.2 ± 4.5ab      | 6.9 ± 2.4c       | 6.2 ± 1.4cd | 0.1 ± 0.02bc                     |
| ZnO NPs   | 17.0 ± 3.6a       | 4.8 ± 1.8b       | 7.0 ± 1.7bd | 0.09 ± 0.03bc                    |
| Bulk ZnO  | 18.6 ± 4.0a       | 6.7 ± 1.8c       | 5.9 ± 1.0ac | 0.11 ± 0.02c                     |

Data are average of 5 replicates from at least three independent growth studies each containing 15 plants. Different letters following each value represent significant differences between the treatments for each growth response ( $p = 0.05$ )

from the CuO NPs were identical (data not shown) and precluded differentiation between these two phases. The remainder of the spectrum ( $36 \pm 10\%$ ) was consistent with the Cu(I)-sulfide standard ( $\chi^2$  of the LC fit = 0.017). Using any other of the standards in Fig. 4a as an end member in addition to the CuO NPs spectrum resulted in a significantly lower quality of the LC fit ( $\chi^2 > 0.1$ ). Although EXAFS data could not be obtained to confirm Cu(I)-S coordination due to the low concentration of Cu in the shoots, the previously described sensitivity of Cu XANES to Cu(I)-S versus

Cu(I)-O coordination (Manceau and Matynia 2010; Pokrovsky et al. 2012) allowed the establishment of Cu(I)-S species both by the results of the LC fits and by the greater similarity of the XANES derivative to Cu<sub>2</sub>S relative to Cu<sub>2</sub>O (derivative not shown).

The Zn XANES measurements are shown in Fig. 4b. The spectrum of the ZnO NP-exposed shoots was significantly different than that of the starting ZnO NPs and was closest to that of a Zn-phosphate standard [hopeite, Zn<sub>3</sub>(PO<sub>4</sub>)<sub>2</sub>·4H<sub>2</sub>O]. Some features in the post-edge region of the XANES (noted by arrows) were

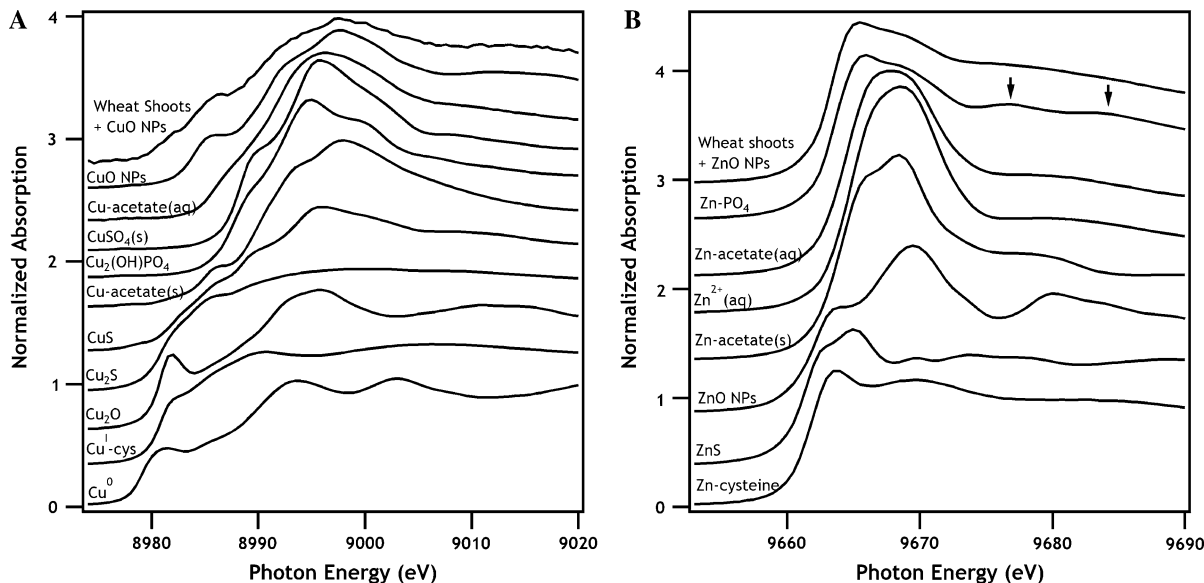


**Fig. 4** Copper and zinc K-edge XANES spectra of wheat shoots from plants grown in a sand matrix amended with CuO and ZnO NPs. **a** The spectrum for Cu in wheat shoots exposed to CuO NPs is compared to spectra for the commercial CuO NPs, aqueous Cu-acetate (Cu-acetate(aq)), Cu-sulfate salt (CuSO<sub>4</sub>(s)), copper hydroxyphosphate (Cu<sub>2</sub>(OH)PO<sub>4</sub>), Cu acetate salt (Cu-acetate(s)), Cu monosulfide (CuS), Cu<sup>I</sup> sulfide

(Cu<sub>2</sub>S), Cu<sup>I</sup> oxide (Cu<sub>2</sub>O), Cu precipitated from Cu<sup>II</sup> and reacted with cysteine (Cu<sup>I</sup>-cys), and Cu metal (Cu<sup>0</sup>). **b** The zinc K-edge XANES spectrum of wheat shoots exposed to ZnO NPs compared with spectra from standards of Zn<sub>3</sub>(PO<sub>4</sub>)<sub>2</sub>·4H<sub>2</sub>O (Zn-PO<sub>4</sub>), aqueous zinc acetate, aqueous Zn<sup>2+</sup> (pH 3.5), ZnO NPs, zinc sulfide (ZnS) and aqueous zinc cysteine

more pronounced in the standard than in the shoots' spectrum. The EXAFS data from the shoots sample also were similar in phase and shape to that from the hopeite standard, but the wheat shoots data show a larger amplitude of the Fourier transform (FT) peaks corresponding to the Zn–O and Zn–P coordination (data not shown). The dissimilarities in the XANES and EXAFS suggested a slightly different coordination environment of the Zn ions in the shoots than Zn in hopeite. The Zn ions in hopeite reside in both tetrahedral and octahedral sites, and the two sites are coordinated by different number of phosphate groups at slightly different distances (Hill and Jones 1976). The spectral differences were therefore rationalized by assuming adsorption of Zn ions to phosphoryl groups in the shoots rather than incorporation into the three-dimensional structure of a Zn-phosphate precipitate.

**Role of dissolved Cu and Zn ions in the phytotoxicity of CuO and ZnO NPs**

As CuO and ZnO NPs released soluble Cu and Zn in the sand over the time period that plant growth was tested, the role of Cu and Zn ions in the phytotoxicity of the NPs was evaluated. Figure 5 shows that shoot length was statistically unaffected by both Cu and Zn ions. However, compared to control plants, root length was significantly ( $p = 0.05$ ) affected by Cu ions but not by Zn ions. The Cu ions significantly ( $p = 0.05$ ) induced root proliferation compared to control and Zn ion treatments. Thus, plant biomass was significantly different ( $p = 0.05$ ) in the presence of Cu ion but not in Zn ion treatment (Fig. 5).

**Induction of root membrane peroxidation and leaf chlorophyll loss by NPs**

Growth of wheat in the presence of CuO NPs, and to a lesser extent ZnO NPs, increased lipid peroxidation in the root membranes as shown by the higher MDA values in extracts from plants grown with the NPs than from the control plants (Table 3). The chlorophyll levels in leaves were decreased in the plants grown with CuO and ZnO NPs compared to control levels in the shoots from the control plants (Table 3).

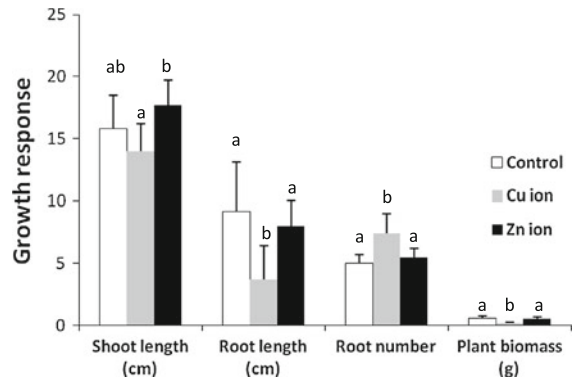


**Fig. 5** Effect on wheat growth in sand of Cu ions (3 mg Cu/kg) and Zn ions (7 mg Zn/kg) equivalent to the highest concentrations of dissolved Cu and Zn released from the CuO and ZnO products in sand over 14-day period. Data are average of 5 replicates from at least two independent growth studies each containing 15 plants in total. Different letters on bars represent significant differences between the treatments for each growth response ( $p = 0.05$ )

**Table 3** Enhanced metal-induced reactive oxygen species-related stress in plants grown in the presence of CuO and ZnO nanoparticles (NPs)

| Treatment | Oxidative stress indicator |                                    |
|-----------|----------------------------|------------------------------------|
|           | MDA ( $\mu\text{M/g FW}$ ) | Chlorophyll ( $\mu\text{g/g FW}$ ) |
| Control   | 1.20 $\pm$ 0.4a            | 15.3 $\pm$ 0.5c                    |
| CuO NPs   | 4.45 $\pm$ 0.4b            | 9.5 $\pm$ 1.4b                     |
| ZnO NPs   | 2.27 $\pm$ 0.2c            | 9.6 $\pm$ 2.0b                     |

Root membrane peroxidation (MDA) and leaf chlorophyll loss in the NP-treated plants are indicated. Different letters after values represent significant differences among the treatments ( $p = 0.05$ ) in each column. FW fresh weight

**Alteration of antioxidative responses of wheat by NPs**

On the basis of the lipid peroxidation observed in plants exposed to the NPs, plant antioxidative responses were evaluated. Root extracts from plants grown with the CuO NPs had higher POD and CAT activities than the extracts from the control plants (Fig. 6a). Plants grown with ZnO NPs had reduced CAT activity (Fig. 6a). More glutathione was present as the oxidized form, GSSG, in the roots than the shoots of the control plants on a fresh weight basis (Fig. 6b). The level of GSSG in the shoots of plants grown with NPs significantly increased ( $p = 0.05$ ) compared to control plants (Fig. 6b). Increases in

GSSG in roots were not significant. IAA oxidase was more active in the root extracts than the shoot extracts of control plants. Figure 6c shows that there was more residual IAA in the reaction mixtures after incubation with extracts from shoots compared with roots. Growth with CuO and ZnO NPs increased IAA oxidase activity in the shoot extracts but had no significant effect on activities in root extracts (Fig. 6c).

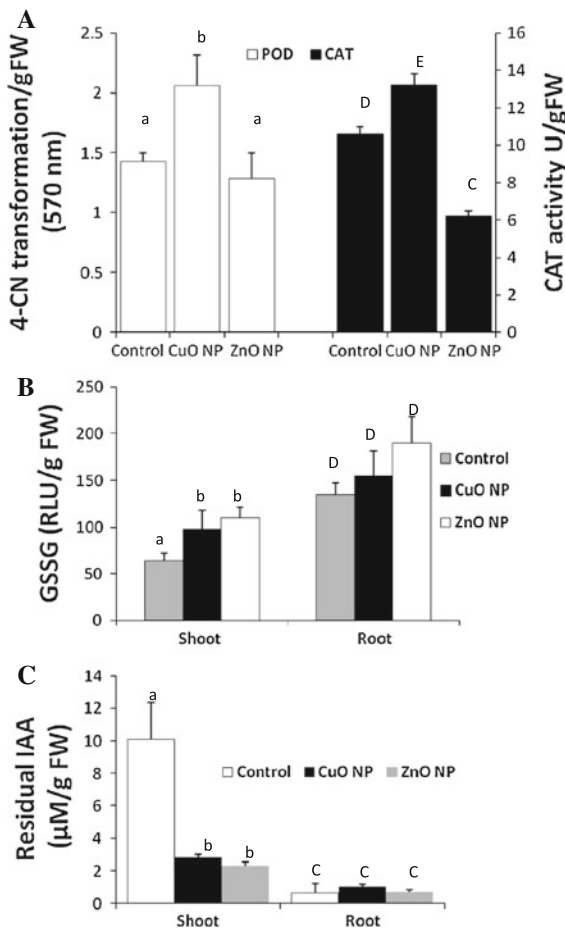


**Fig. 6** Effects of CuO and ZnO NPs on systems that regulate oxidative stress *in planta*. **a** Peroxidase (POD) activity measured by absorbance at 570 nm due to transformation of 4-chloronaphthol (4-CN) and catalase (CAT) activity in root extracts from wheat plants grown with and without exposure to CuO and ZnO NPs. **b** Levels of oxidized glutathione (GSSG) in extracts from roots and shoots of plants grown with and without exposure to CuO and ZnO NPs. **c** Assessment of IAA oxidase activity in extracts from wheat shoots and roots grown with and without exposure to CuO and ZnO NPs. Different letters on bars represent significant differences ( $p = 0.05$ ) in each figure, differently for POD and CAT assays (**a**) and differently for root and shoot samples (**b**, **c**). RLU relative light unit

## Discussion

We demonstrate in this study that commercial CuO and ZnO NPs released soluble Cu and Zn in a sand matrix, with the particles present in the sand as NPs and NP aggregates. The extent of aggregation might have been influenced by the presence of Si and P oxyanions present from the sand and as impurities in the NPs. Such anions would affect particle surface charge, leading to changes in the biological responses to the NPs. Liu et al. (2011) demonstrated the impact of Si and P oxyanions on the point of zero charge (PZC) of  $\text{TiO}_2$ . The PZC decreased with increasing concentrations of Si and P present as contaminants in several commercial preparations of  $\text{TiO}_2$ . Despite aggregation, the CuO NPs inhibited wheat growth and changed root structure when the plants were grown in the sand matrix. Our studies in sand confirmed the inhibition by ZnO NPs of wheat growth in an agricultural soil recently described by Du et al. (2011). The larger size of NP aggregates shown by DLS than by AFM in water suspensions of the NPs could be attributed to factors inherent in DLS-based analysis (see also Montes-Burgos et al. 2010). Mixing with wetted sand promoted structural rearrangements of the ZnO NPs to elongated particles approaching micron size, whereas most of the aggregated particles of CuO NPs retained a round appearance. The factors from the sand that contributed to the change in morphology of the ZnO NPs discussed below are under further study.

Concentrations of Ca, Mg, or Na and organic matter in the sand were too low to influence aggregation of the NPs. Previously, we showed that aggregation to micron sizes of these NPs in aqueous suspensions did not eliminate their ability to alter metabolism in soil bacteria (Dimkpa et al. 2011b; Gajjar et al. 2009). Despite aggregation, the particles released ions into the wetted sand. However, the ion release levels decreased with time, and we suggest that increased aggregation may have reduced the dissolution of the NPs. We speculate that the morphological change in the ZnO NPs in the sand was due to a mineral transformation of ZnO. Both the observed morphology in AFM (Fig. 2) and the decrease in Zn solubilization with time were consistent with precipitation of hydrozincite [ $\text{Zn}_5(\text{CO}_3)_2(\text{OH})_6$ ] in a solution with a pH of 7.9 and in equilibrium with ambient  $\text{CO}_2$  (Ghose 1964; Preis and Gamsjäger 2001).

Transformation of ZnO to secondary phases in contaminated soil has been found previously (Voegelin et al. 2005), and may provide an important control on the fate of ZnO NPs. As discussed by Du et al. (2011) in their soil studies with ZnO NPs, the NPs used here acted as sources of soluble metal. Although metal solubilization varied between NPs and the bulk particles initially, overall release levels were similar over time.

The levels of metals released from the CuO and ZnO products were far below the levels of Cu and Zn ions reported to be phytotoxic to wheat and other plant species in a sand matrix: 120 mg/l Cu (in wheat), and 82–214 mg/l Zn (in forbs species) (Paschke and Redente 2002; Paschke et al. 2006). Many of our observations correlated with similar findings occurring with Cu or Zn ion treatments, and generally supported the greater toxicity of Cu than Zn (Warne et al. 2008). For instance, the proliferation of lateral roots observed with the NPs, bulk CuO and Cu ions (data not shown) agreed with this being a common plant response to metal stress at toxic levels (Potters et al. 2007 and references therein).

We observed that the commercial NP products caused oxidative stress (root lipid peroxidation, decreased chlorophyll levels in shoots, increased GSSG) agreeing with reported changes caused by both NPs and metal ion treatments. Zn ions ( $\approx 14$ – $13,600$  mg/l, as  $\text{ZnCl}_2$ ) induced free radical formation in wheat, resulting in increased MDA and lower levels of reduced glutathione (GSH) (Panda et al. (2003) and reduced chlorophyll contents (Aarti et al. 2006). The role of GSH as a major protectant against ROS (Apel and Hirt 2004; Pompella et al. 2003; Sies 1999) agreed with our finding of higher levels of GSSG in the NP-exposed plants. Our results also supported that roots have higher GSH levels than shoots as previously discussed by Zaets et al. (2010). Increased production of enzymes to counteract oxidative stress, CAT and POD activities, as we observed with CuO NP treatment, occurred with exposure to Cu ions ( $\approx 12$  mg/l, on the basis of anhydrous  $\text{CuSO}_4$ ) in hydroponic conditions (Gajewska and Sklodowska 2010). The lack of an increase in CAT or POD activities with ZnO NPs agreed with the non-responsiveness of these enzymes to Zn ions in wheat (Panda et al. 2003). Hernandez-Viezcas et al. (2011) also reported no increase in CAT activity by treatments with ZnO NPs at 500 mg/l in hydroponically grown

mesquite; activity was increased at 4,000 mg/l. Plant growth in soil polluted with an array of different heavy metals, including Cu (50 mg/kg) and Zn (72 mg/kg) (Dimkpa et al. 2009) and in vitro growth with Cu ions (Chaoui and El-Ferjani 2005) increased IAA oxidase activity as we observed with the NP-exposed plants. The changes in chlorophyll levels also agreed with studies of NP treatments in hydroponic conditions: reduced chlorophyll levels occurred with core-shell CuO NPs ( $\approx 10$ – $20$  mg/l) in the green alga, *Chlamydomonas reinhardtii* (Saison et al. 2010) and CuO NPs (400 mg/l) in *Lemna gibba* plants (Perreault et al. 2010). It is difficult to extrapolate the extent to which metal ions released from the NPs caused the changes to plant growth we observed with the NPs. The reduced root growth and biomass seen with the Cu ion treatment suggested that this was instrumental in the plants' response to the CuO NPs. The Zn ions did not duplicate the responses. However, for both NPs, we postulate that increased oxidative stress, and possibly decreased IAA levels due to enhanced IAA oxidase (Potters et al. 2007), contributed to impaired wheat growth.

We deduced that the findings of altered shoot metabolism correlated with abnormal accumulations of these metals (for Cu 20-fold and for Zn 24-fold above control) when plants were grown with NPs. Wheat meristematic tissues have a high requirement for Zn and its translocation is effective (Haslett et al. 2001), such that Zn is better accumulated in shoots in comparison to Cu (Haslett et al. 2001; Page and Feller 2005). Other plants species also accumulate large amounts of Zn in aerial parts (Hernandez-Viezcas et al. 2011; Paschke et al. 2006; Qu et al. 2011).

The XANES data showed that CuO was detected in the shoots of wheat seedlings grown from roots exposed to the CuO NPs. Using LC analysis of the XANES spectra from plants grown with CuO NPs, we found that the majority ( $64 \pm 10$  %) of the Cu was in the original form as CuO and the rest ( $36 \pm 10$  %) was bound to sulfur as a reduced Cu(I)–S species. Similarly, previous XANES analysis with the Cu-tolerant plant *Elsholtzia splendens* indicated that most Cu in shoots was divalent when the plant was provided with Cu ions (Shi et al. 2008). Recent stable isotope studies suggested that reduction of Cu in the plants to Cu(I) was part of the normal uptake process (Jouvin et al. 2012). Whether the CuO NPs were transported into the wheat shoot or formed from dissolved Cu ions

taken into the plant from the roots requires further investigation. However, given that freshly precipitated  $\text{Cu}(\text{OH})_2$  must be heated to form CuO NPs (Haiming et al. 2004; Topnani et al. 2009), we speculated that the presence of CuO in the plants was due to uptake and transport, rather than formation of novel NPs *in planta*. The finding of CuO in wheat shoot agreed with detection of intact NPs of Cu,  $\text{Ni}(\text{OH})_2$ ,  $\text{CeO}_2$ , and  $\text{Fe}_3\text{O}_4$  within plant tissues in mung bean, wheat, mesquite, cucumber, and pumpkin (Lee et al. 2008; Parsons et al. 2010; Zhang et al. 2011; Zhu et al. 2008). Navarro et al. (2008) hypothesized that the attachment of NPs to plant cells induced changes leading to the potential transport of even more NPs into the cells. Sites of localized damage were observed in the roots exposed to CuO NPs as darkened lesions.

In contrast, shoots from the ZnO NP-grown plants contained a Zn species different from the original ZnO NPs. The XANES spectrum of shoots of these plants was closest to the spectrum of Zn-phosphate standard of the mineral hopeite [ $(\text{Zn}_3(\text{PO}_4)_2 \cdot 4\text{H}_2\text{O})$ ], indicating solubilization from the ZnO NPs was involved. The difference in response between the solubility of the ZnO and the transport of CuO NPs into shoots relates to the difference in solubility: ZnO (zincite) has a greater solubility,  $\log K = 11.16$ , compared to  $\log K = 7.66$  for CuO (tenurite) (Lindsay 1979). Slight differences in the XANES spectrum of the shoot sample and the phosphate mineral were present (arrows in Fig. 4b). The differences are likely related to differences between Zn binding in the mineral standard and adsorption to phosphoryl functional groups and ligands such as phytic acid in the wheat plants (Vansteveninck et al. 1994). The transformation of the ZnO NPs to Zn-phosphate agreed with previous reports for *Arabidopsis halleri* (Sarret et al. 2002); transformation of ZnO NPs to Zn ions was observed in soybean and mesquite plants (Hernandez-Viezcas et al. 2011; López-Moreno et al. 2010). Our results with wheat differ from those of Lin and Xing (2008), where little Zn was detected in shoots of hydroponically grown perennial ryegrass treated with 1,000 mg/l ZnO NPs, despite identifying intact ZnO NPs at damage sites in the roots.

Although accumulation of metals at toxic levels in plants are harmful for the food chain, their uptake from NPs could permit phytoremediation of soils contaminated with NPs, or the actual mining for precious metals such as silver and gold (Haverkamp and Marshall 2009). Also, metal loading from NPs could

remedy deficiencies in Zn and Cu in metal-deficient soils (Alloway 2009; Nair et al. 2010; White and Broadley 2009). However, our studies were performed in sand where there was no organic matter or materials of high ionic strength that could alter NP stability and transport likely to occur in soil (Lin et al. 2010). Thus, the extent to which such factors would influence uptake into plants in soil awaits investigation.

In summary, we demonstrated that CuO and ZnO NPs in a sand growth matrix aggregated into large particles, with evolution of structure for the ZnO NPs. The NPs impaired plant growth more than bulk particles, although both products (NPs and bulks) caused similar accumulation of the respective metals, Cu and Zn, within wheat shoots. The Zn in the shoots was complexed with phosphoryl moieties, implying that dissolution of the ZnO NPs was important in the plant. In contrast, CuO and lower levels of Cu(I)-sulfur complexes were detected in shoot after growth with CuO NPs. The Cu(I)-sulfur complex was consistent with Cu release from the NPs and its reduction by plant processes. Impaired root growth could be a consequence of dissolved Cu from the NPs. Dissolved Cu and Zn also could be the cause of the oxidative stress observed in the wheat seedlings grown with both CuO and ZnO NPs. How these toxic effects may be modified in soil by mineral complexation and transformation of NPs that could not occur in the sand matrix awaits further chemical, physiological, and biological evaluations.

**Acknowledgments** This work was supported by the United States Department of Agriculture (USDA-CSREES) Grant 2009-35603-05037, the Utah Agricultural Experiment Station (Journal Paper # 8261), and the Utah Water Research Laboratory. Thanks to Moon-Juin Ngooi and Jordan Goodman for help with plant growth. For XANES data acquisition, we would like to thank John Katsoudas and Edward Lang for support at the MRCAT/EnviroCAT Sector 10BM beamline. Ken Kemner and Bhoopesh Mishra are thanked for their helpful input regarding the XAS and for help at the beamline. MRCAT operations are supported by U.S. Department of Energy (DOE) and the MRCAT member institutions. Use of the Advanced Photon Source, an Office of Science User Facility operated for the DOE Office of Science by Argonne National Laboratory, is supported by the DOE under Contract No. DE-AC02-06CH11357.

## References

- Aarti PD, Tanaka R, Tanaka A (2006) Effects of oxidative stress on chlorophyll biosynthesis in cucumber (*Cucumis sativus*) cotyledons. *Physiol Plantarum* 128:186–197

- Akiyama M, Watanabe Y, Nishikawa T (1989) Peroxidase-activity in mast-cell granules in *Urticaria pigmentosa*. *Dematologica* 178:145–150
- Alloway BJ (2009) Soil factors associated with zinc deficiency in crops and humans. *Environ Geochem Health* 31:537–548
- Apel K, Hirt H (2004) Reactive oxygen species: metabolism, oxidative stress and signal transduction. *Annu Rev Plant Biol* 55:373–399
- Asli S, Neumann PM (2009) Colloidal suspensions of clay or titanium dioxide nanoparticles can inhibit leaf growth and transpiration via physical effects on root water transport. *Plant Cell Environ* 32:577–584
- Atha DH, Wang H, Petersen EJ, Cleveland D, Holbrook RD, Jaruga P, Dizdaroglu M, Xing B, Nelson BC (2012) Copper oxide nanoparticle mediated DNA damage in terrestrial plant models. *Environ Sci Technol* 46:1819–1827
- Barrena R, Casals E, Colon J, Font X, Sanchez A, Puntès V (2009) Evaluation of the ecotoxicity of model nanoparticles. *Chemosph* 75:850–857
- Cakmak I, Horst WJ (1991) Effect of aluminum on liquid peroxidation, superoxide dismutase catalysis and peroxidase activities in root tips of soybean *Glycine max*. *Physiol Plantarum* 83:463–468
- Chaoui A, El-Ferjani E (2005) Effects of cadmium and copper on antioxidant capacities, lignification and auxin degradation in leaves of pea (*Pisum sativum* L.) seedlings. *Comptes Rendus Biol* 328:23–31
- Dimkpa C, Merten D, Svatoš A, Büchel G, Kothe E (2008) Hydroxamate siderophores produced by *Streptomyces acidiscabies* E13 bind nickel and promote growth in cowpea (*Vigna unguiculata* L.) under nickel stress. *Can J Microbiol* 54:163–172
- Dimkpa CO, Merten D, Svatoš A, Büchel G, Kothe E (2009) Metal-induced oxidative stress impacting plant growth in contaminated soil is alleviated by microbial siderophores. *Soil Biol Biochem* 41:154–162
- Dimkpa CO, Calder C, Gajjar P, Merugu S, Huang W, Britt DW, McLean JE, Johnson WP, Anderson AJ (2011a) Interaction of silver nanoparticles with an environmentally beneficial bacterium, *Pseudomonas chlororaphis*. *J Hazard Mater* 188:428–435
- Dimkpa CO, Calder A, McLean JE, Britt DW, Anderson AJ (2011b) Responses of a soil bacterium, *Pseudomonas chlororaphis* O6 to commercial metal oxide nanoparticles compared with responses to metal ions. *Environ Pollut* 159:1749–1756
- Dimkpa CO, McLean JE, Britt DW, Anderson AJ (2012a) CuO and ZnO nanoparticles differently affect the secretion of fluorescent siderophores in the beneficial root colonizer, *Pseudomonas chlororaphis* O6. *Nanotoxicology* 6:635–642
- Dimkpa CO, Zeng J, McLean JE, Britt DW, Zhan J, Anderson AJ (2012b) Production of indole-3-acetic acid via the indole-3-acetamide pathway in the plant-beneficial bacterium, *Pseudomonas chlororaphis* O6 is inhibited by ZnO nanoparticles but enhanced by CuO nanoparticles. *Appl Environ Microbiol* 78:1404–1410
- Dimkpa CO, McLean JE, Britt DW, Johnson WP, Arey B, Lea SA, Anderson AJ (2012c) Nano-specific inhibition of pyoverdine siderophore production in *Pseudomonas chlororaphis* O6 by CuO nanoparticles. *Chem Res Toxicol* 25:1066–1074
- Du W, Sun Y, Ji R, Zhu J, Wu J, Guo H (2011) TiO<sub>2</sub> and ZnO nanoparticles negatively affect wheat growth and soil enzyme activities in agricultural soil. *J Environ Monit* 13:822–828
- Gajewska E, Sklodowska M (2010) Differential effect of equal copper, cadmium and nickel concentration on biochemical reactions in wheat seedlings. *Ecotoxicol Environ Safety* 73:996–1003
- Gajjar P, Pettee B, Britt DW, Huang W, Johnson WP, Anderson AJ (2009) Antimicrobial activities of commercial nanoparticles against an environmental soil microbe, *Pseudomonas putida* KT2440. *J Biol Eng* 3:9
- Gao FQ, Hong FH, Liu C, Zheng L, Su MY, Wu X, Yang F, Wu C, Yang P (2006) Mechanism of nano-anatase TiO<sub>2</sub> on promoting photosynthetic carbon reaction of spinach—inducing complex of rubisco–rubisco activase. *Biol Trace Element Res* 111:239–253
- Gao F, Liu C, Qu C, Zheng L, Yang F, Su M, Hong F (2008) Was improvement of spinach growth by nano-TiO<sub>2</sub> treatment related to the changes of rubisco activase? *Biometals* 21:211–217
- Ghose S (1964) The crystal structure of hydrozincite, Zn<sub>5</sub>(OH)<sub>6</sub>(CO<sub>3</sub>)<sub>2</sub>. *Acta Crystallogr A* 17:1051–1057
- Haiming F, Lintao Y, Wenshen H, Xingfang W, Zhenyu W, Sishen X, Bingsuo Z (2004) Controlled synthesis of monodispersed CuO nanocrystals. *Nanotechnol* 15:37
- Haslett BS, Reid RJ, Rengel Z (2001) Zinc mobility in wheat: uptake and distribution of zinc applied to leaves or roots. *Ann Bot* 87:379–386
- Haverkamp RG, Marshall AT (2009) The mechanism of metal nanoparticle formation in plants: limits on accumulation. *J Nanopart Res* 11:1453–1463
- Hernandez-Viezcas JA, Castillo-Michel H, Servin AD, Peralta-Videa JR, Gardea-Torresdey JL (2011) Spectroscopic verification of zinc absorption and distribution in the desert plant *Prosopis juliflora-velutina* (velvet mesquite) treated with ZnO nanoparticles. *Chem Eng J* 170:346–352
- Hill RJ, Jones JB (1976) Crystal-structure of hopeite. *Am Mineral* 61:987–995
- Jouvin D, Weiss DJ, Mason TFM, Bravin MN, Louvat P, Zhao F, Ferec F, Hinsinger P, Benedetti MF (2012) Stable isotopes of Cu and Zn in higher plants: evidence for Cu reduction at the root surface and two conceptual models for isotopic fractionation processes. *Environ Sci Technol* 46:2652–2660
- Kau LS, Spira-Solomon DJ, Penner-Hahn JE, Hodgson KO, Solomon EI (1987) X-ray absorption edge determination of the oxidation state and coordination number of copper. Application to the type 3 site in *Rhus vernicifera* laccase and its reaction with oxygen. *J Am Chem Soc* 109:6433–6442
- Kim JY, Rodriguez JA, Hanson JC, Frenkel AI, Lee PL (2003) Reduction of CuO and Cu<sub>2</sub>O with H<sub>2</sub>: H embedding and kinetic effects in the formation of suboxides. *J Am Chem Soc* 125:10684–10692
- Kropf AJ, Katsoudas J, Chattopadhyay S, Shibata T, Lang EA, Zyryanov VN, Ravel B, McIvor K, Kemner KM, Scheckel KG, Bare SR, Terry J, Kelly SD, Bunker BA, Segre CU (2010) The new MRCAT (Sector 10) bending magnet

- beamline at the advanced photon source. AIP Conf Proc 1234:299–302
- Lee WM, An YJ, Yoon H, Kweon HS (2008) Toxicity and bioavailability of copper nanoparticles to the terrestrial plants mung bean (*Phaseolus radiatus*) and wheat (*Triticum aestivum*): plant agar test for water-insoluble nanoparticles. Environ Toxicol Chem 27:1915–1921
- Lee WL, Mahendra S, Zodrow K, Li D, Tsai YC, Braam J, Alvarez PJJ (2010) Developmental phytotoxicity of metal oxide nanoparticles to *Arabidopsis thaliana*. Environ Toxicol Chem 29:669–675
- Lin DH, Xing BS (2007) Phytotoxicity of nanoparticles: inhibition of seed germination and root growth. Environ Pollut 150:243–250
- Lin DH, Xing BS (2008) Root uptake and phytotoxicity of ZnO nanoparticles. Environ Sci Technol 42:5580–5585
- Lin D, Tian X, Wu F, Xing B (2010) Fate and transport of engineered nanomaterials in the environment. J Environ Qual 39:1896–1908
- Lindsay WL (1979) Chemical equilibrium in soils. Wiley, New York
- Liu X, Chen G, Su C (2011) Effects of material properties on sedimentation and aggregation of titanium dioxide nanoparticles of anatase and rutile in the aqueous phase. J Colloid Interface Sci 363:84–91
- López-Moreno ML, de la Rosa G, Hernández-Viezcás JA, Castillo-Michel H, Botez CE, Peralta-Videa JR, Gardea-Torresdey JL (2010) Evidence of the differential biotransformation and genotoxicity of ZnO and CeO<sub>2</sub> nanoparticles on soybean (*Glycine max*) plants. Environ Sci Technol 44:7315–7320
- Manceau A, Matynia A (2010) The nature of Cu bonding to natural organic matter. Geochim Cosmochim Acta 74:2556–2580
- Márquez-García B, Córdoba F (2009) Antioxidative system and oxidative stress markers in wild populations of *Erica australis* L. differentially exposed to pyrite mining activities. Environ Res 109:968–974
- Montes-Burgos I, Walczyk D, Patrick H, Smith J, Lynch I, Dawson K (2010) Characterization of nanoparticle size and state prior to nanotoxicological studies. J Nanopart Res 12:47–53
- Nair R, Varghese SH, Nair NG, Maekawa T, Yoshida Y, Kumar DS (2010) Nanoparticulate material delivery to plants. Plant Sci 179:154–163
- Navarro E, Baun A, Behra R, Hartmann NB, Filser J, Miao AJ, Quigg A, Santschi PH, Sigg L (2008) Environmental behavior and ecotoxicity of engineered nanoparticles to algae, plants, and fungi. Ecotoxicol 17:372–386
- Newville M (2001) IFEFFIT: interactive XAFS analysis and FEFF fitting. J Synchrotron Radiat 8:322–324
- Page V, Feller U (2005) Selective transport of zinc, manganese, nickel, cobalt and cadmium in the root system and transfer to the leaves in young wheat plants. Ann Bot 96:425–434
- Pal S, Tak YK, Song JM (2007) Does the antibacterial activity of silver nanoparticles depend on the shape of the nanoparticle? A study of the gram-negative bacterium *Escherichia coli*. Appl Environ Microbiol 73:1712–1720
- Panda SK, Chaudhury I, Khan MH (2003) Heavy metals induce lipid peroxidation and affect antioxidants in wheat leaves. Biol Plantarum 46:289–294
- Parsons JG, Lopez ML, Gonzalez CM, Peralta-Videa JR, Gardea-Torresdey JL (2010) Toxicity and biotransformation of uncoated and coated nickel hydroxide nanoparticles on mesquite plants. Environ Toxicol Chem 29:1146–1154
- Paschke MW, Redente EF (2002) Copper toxicity thresholds for important restoration grass species of the Western United States. Environ Toxicol Chem 21:2692–2697
- Paschke MW, Perry LG, Redente EF (2006) Zinc toxicity thresholds for reclamation forb species. Water Air Soil Pollut 170:317–330
- Perreault F, Ouakroum A, Pirastru L, Sirois L, Matias WG, Popovic R (2010) Evaluation of copper oxide nanoparticles toxicity using chlorophyll *a* fluorescence imaging in *Lemna gibba*. J Bot 763142
- Pokrovsky OS, Pokrovski GS, Shirokova LS, Gonzalez AG, Emnova EE, Feurtet-Mazel A (2012) Chemical and structural status of copper associated with oxygenic and anoxygenic phototrophs and heterotrophs: possible evolutionary consequences. Geobiol 10:130–149
- Pompella A, Visvikis A, Paolicchi A, De Tata V, Casini AF (2003) The changing faces of glutathione, a cellular protagonist. Biochem Pharmacol 66:1499–1503
- Potters G, Pasternak TP, Guisez Y, Palme KJ, Jansen MAK (2007) Stress-induced morphogenic responses: growing out of trouble? Trends Plant Sci 12:98–105
- Preis W, Gamsjäger H (2001) Solid + solute phase equilibria in aqueous solution. XIII. Thermodynamic properties of hydrozincite and predominance diagrams for (Zn<sup>2+</sup> + H<sub>2</sub>O + CO<sub>2</sub>). The J Chem Thermodynamics 33:803–819
- Qu J, Yuan X, Wang X, Shao P (2011) Zinc accumulation and synthesis of ZnO nanoparticles using *Physalis alkekengi* L. Environ Pollut 159:1783–1788
- Ravel B, Newville M (2005) ARTEMIS, HEPHAESTUS: data analysis for X-ray absorption spectroscopy using IFEFFIT. J Synchrotron Radiat 12:537–541
- Saison C, Perreault F, Daigle JC, Fortin C, Claverie J, Morin M, Popovic R (2010) Effect of core-shell copper oxide nanoparticles on cell culture morphology and photosynthesis (photosystem II energy distribution) in the green alga, *Chlamydomonas reinhardtii*. Aquatic Toxicol 96:109–114
- Sarret G, Laprade PS, Bert V, Proux O, Hazemann JL, Traverse A, Marcus MA, Manceau A (2002) Forms of zinc accumulated in the hyperaccumulator *Arabidopsis halleri*. Plant Physiol 130:1815–1826
- Shi J, Wu B, Yuan X, YY C, Chen X, Chen Y, HU T (2008) An X-ray absorption spectroscopy investigation of speciation and biotransformation of copper in *Elsholtzia splendens*. Plant Soil 302:163–174
- Sies H (1999) Glutathione and its role in cellular functions. Free Radic Biol Med 27:916–921
- Stampoulis D, Sinha SK, White JC (2009) Assay-dependent phytotoxicity of nanoparticles to plants. Environ Sci Technol 43:9473–9479
- Stern EA, Heald SM (1979) X-ray filter assembly for fluorescence measurements of x-ray absorption fine-structure. Rev Sci Instrum 50:1579–1582
- Tait MA, Hik SD (2003) Is dimethylsulfoxide a reliable solvent for extracting chlorophyll under field conditions? Photosynth Res 78:87–91

- Topnani N, Kushwaha S, Athar T (2009) Wet synthesis of copper oxide nanopowder. *Int J Green Nanotechnol* 1:M67–M73
- Vansteveninck RFM, Babare A, Fernando DR, Vansteveninck ME (1994) The binding of zinc, but not cadmium, by phytic acid in roots of crop plants. *Plant Soil* 167:157–164
- Voegelin A, Pfister S, Scheinost AC, Marcus MA, Kretzschmar R (2005) Changes in zinc speciation in field soil after contamination with zinc oxide. *Environ Sci Technol* 39:6616–6623
- Warne MS, Heemsbergen D, Stevens D, McLaughlin M, Cozens G, Whatmuff M, Broos K, Barry G, Bell M, Nash D, Pritchard D, Penney N (2008) Modeling the toxicity of copper and zinc salts to wheat in 14 soils. *Environ Toxicol Chem* 27:786–792
- White PJ, Broadley MR (2009) Biofortification of crops with seven mineral elements often lacking in human diets—iron, zinc, copper, calcium, magnesium, selenium and iodine. *New Phytol* 182:49–84
- Yang L, Watts DJ (2005) Particle surface characteristics may play an important role in the phytotoxicity of alumina nanoparticles. *Toxicol Lett* 158:122–132
- Zaets I, Kramarev S, Kozyrovskam N (2010) Inoculation with a bacterial consortium alleviates the effect of cadmium overdose in soybean plants. *Cent Eur J Biol* 5:481–490
- Zhang ZY, He X, Zhang HF, Zhang P, Ding YY, Zhao YL (2011) Uptake and distribution of ceria nanoparticles in cucumber plants. *Metallomics* 3:816–822
- Zhu H, Han J, Xiao JQ, Jin Y (2008) Uptake, translocation, and accumulation of manufactured iron oxide nanoparticles by pumpkin plants. *J Environ Monit* 10:713–717